SPATIAL-TEMPORAL SURFACE WATER AVAILABILITY IN THE TULANCINGO RIVER BASIN, HIDALGO, MEXICO

Sandra Luz **Torres-Suárez**[1], Martín Alejandro **Bolaños-González**[1*],

Laura Alicia **Ibáñez-Castillo**[2], Abel **Quevedo-Nolasco**[1], Ramón **Arteaga-Ramírez**[2],

Axel Eduardo **Rico-Sánchez**[1], Humberto **Vaquera-Huerta**[1]

[1]Colegio de Postgraduados Campus Montecillo. Posgrado en Hidrociencias. Carretera México-Texcoco km 36.5, Montecillo, Texcoco, State of Mexico, Mexico. C. P. 56264.

[2]Universidad Autónoma Chapingo. Departamento de Irrigación, Posgrado en Ingeniería Agrícola y Uso Integral del Agua. Carretera México-Texcoco km 38.5, Chapingo, Texcoco, State of Mexico, Mexico. C. P. 56227.

* Author for correspondence: bolanos@colpos.mx

ABSTRACT

The Tulancingo River basin is part of the upper Metztitlán River basin and has an aquifer deficiency that covers 87 % of its surface area; however, floods have occurred in the valley region. This disparity encouraged the current work, the goal of which was to estimate the spatio-temporal availability of water in the soil within the basin from the modeling of surface water balance elements. Sensitivity analysis of the model fit parameters was performed with the SWATCUP program and the SUFI2 algorithm. The runoff values were estimated with the SWAT program and were compared with the records of the Venados Hydrometric Station, obtaining values of the statistical indicators $R^2 = 0.89$ and Nash Sutcliffe (NS) = 0.86 for the calibration period (1982–2002); and $R^2 = 0.77$ and NS = 0.62 for the validation period (2003–2013). Of the nine sub-basins that make up the Tulancingo basin, the upper sub-basins of the Río Chico (11), Ventoquipa stream (12), and San Lorenzo River (13) showed values 2.2 times higher than the rainfall depth of the lower sub-basins (5, 6, 7, 8, 9, and 10). Surface runoff and infiltration reported maximum values from July to October and minimum values from April to May. The maximum final water availability in the soil occurred in September. Regarding the analysis by periods, the Generalized Additive Model provided a good fit for most of the variables ($0.6 < R^2 < 0.94$); during the last period, higher values were observed than in the previous periods ($p < 0.001$), identifying a change in the hydrological state of the basin. This was mainly associated with a significant change in rainfall, which was reflected in the trend of surface runoff.

Keywords: water balance, calibration, SWAT, Generalized Additive Model.

INTRODUCTION

The surface area of the Tulancingo River basin is subject to 87 % of the "Decree establishing a ban on the abstraction of groundwater," as it is located within aquifer 1317, "Valle de Tulancingo." This aquifer tripled its average annual water availability deficit in just seven years, from -6.84 to -20.93 hm³ year⁻¹ (DOF, 2020). This situation,

while reflecting the scarcity of groundwater resources within the same region, contrasts with the presence of extreme hydrometeorological events.

Herrera *et al*. (2018) mention that these phenomena are related to the interaction of easterly waves with westerly flow and tropical cyclones from the Gulf of Mexico, mainly from August to October, and have motivated two-dimensional hydraulic modeling to obtain flood risk maps in the city of Tulancingo, such as the one carried out by Bonasia *et al*. (2017). Similarly, Valdez-Lazalde *et al.* (2011), Ortíz-Gómez *et al*. (2015), and Mendoza-Cariño *et al*. (2018) developed basin-wide studies of land use change, water allocation by type of use, and hydrological analysis, down to the Metztitlán River.

These studies present the general conditions of the basin to which the Tulancingo River belongs; however, as they have been oriented towards the analysis of a particular element, runoff or land use and vegetation, without considering the relationship that exists between them or with other elements of the balance (infiltration, base flow, etc.), they do not explain the deficit-excess phenomenon that occurs locally. In this sense, the integration of the elements that constitute the water balance, analyzed geospatially and temporally, can help in the assimilation of the problem of origin, zoning the availability, and planning the management of water resources in a sustainable manner.

In a water balance, the spatio-temporal distribution of precipitation determines the amount of water reaching the land surface; temperature, humidity, and vegetation cover influence the proportion of water evapotranspired; slope and soil characteristics and conditions influence infiltration and runoff (Siad *et al.*, 2019). Thus, soil water storage and availability at the catchment level are influenced by each element, given their interaction and influence.

A large number of hydrological models have been developed to quantify the elements that make up the hydrological cycle at the catchment level. Lopes *et al.* (2021) mention that it is necessary to take into account model factors such as purpose, level of complexity, and availability of information for the selection of the most appropriate model in a study. The Soil and Water Assessment Tool (SWAT) hydrological model has been used and tested in a number of areas, including water balances (Shawul *et al.*, 2019). The evaluation and critical review by Keller *et al.* (2023) of the 21 most widely used hydrological models gave SWAT an "H" (high) rating, highlighting it in terms of functionality, catchment applicability, and scales, among other aspects.

The results provided by such a program have proven to be favorable if sufficient climate data are available to establish a validation and calibration time period (Marín *et al.*, 2020). Given the above, the objective of this study is to quantify spatially and temporally the availability of water in the soil from the water balance in the Tulancingo River basin, identify the areas with availability and deficit, and observe its historical behavior in sub-periods. It was considered that the SWAT model has sufficient capacity and accuracy for this purpose, so that the results obtained can serve as a basis for the implementation of specific measures for the conservation and proper management of water resources at the basin level.

MATERIALS AND METHODS

The Tulancingo River rises at the border of the states of Hidalgo and Puebla, crosses the valley and the city of the same name in a north-westerly direction, continues its course as the Alcholoya River, and finally receives the name of Metztitlán within Hydrological Region 26 "Río Pánuco." The modeling of the basin, which was carried out with the help of the SWAT program, covers the basin from its origin to the hydrometric station 26024 "Venados" on the Metztitlán River, at coordinates 20° 28' 2.38" N and 98° 40' 15.52" W. Information for calibration and validation is available at this site. The Tulancingo basin (Figure 1) is indicated as having its outlet at coordinates 20° 10' 36.3" N and 98° 22' 28.19" W.
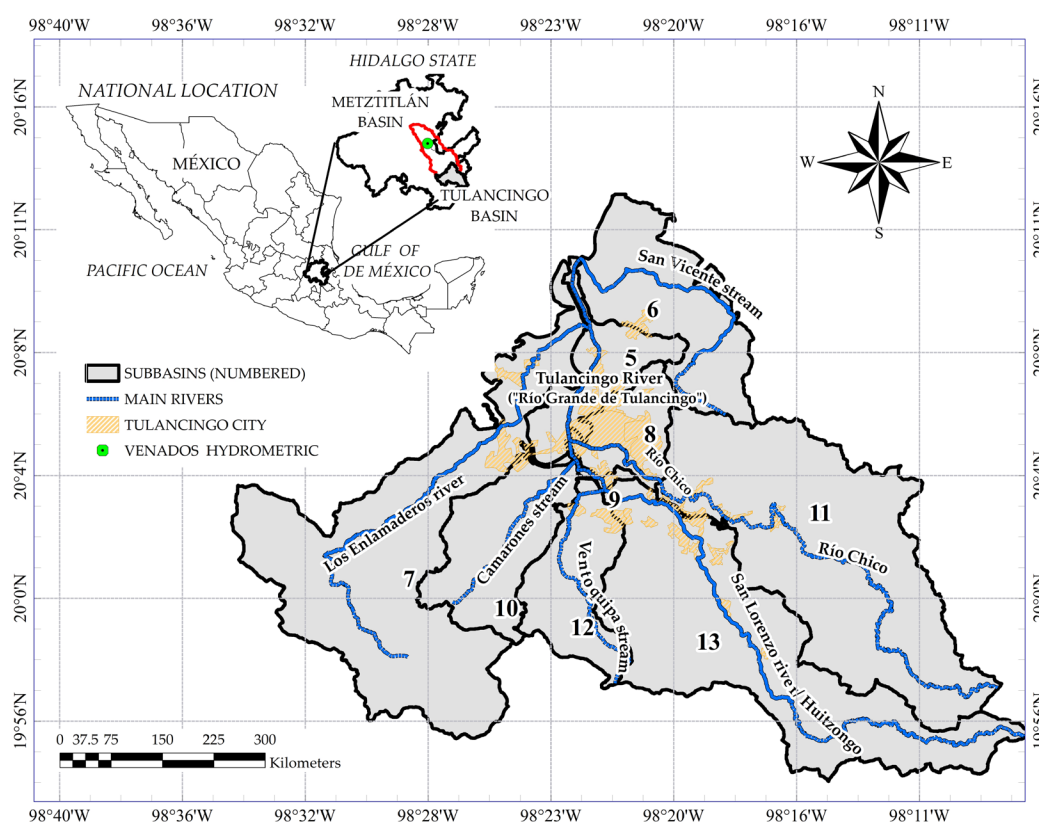
Figure 1. Geographic coordinates for the Tulancingo basin's sub-basins and main streams (INEGI, 2014).

After calibrating using hydrometric data 83 km downstream, the considerations made to the model described below in the input data were applied to the Venados catchment, with output at the hydrometric station. The representation, quantification of hydrological balance elements, and analysis carried out for the Tulancingo basin

reflect the most realistic condition possible for its surface area, which covers almost 40 % of the total area (733 out of 1953 km^2).

Model input data

Weather information

Daily precipitation and temperature data from nine meteorological stations within the watershed were included, covering a 38-year period (1980–2017). Missing data estimation was performed using the U.S. National Weather Service method (Ramírez-Cruz *et al*., 2015), which is an average obtained with the inverse of the squared distance as the weighting factor. Solar radiation, dew point temperature, and wind speed values were obtained with the help of the Climate Forecast System Reanalysis (CFSR) (Table 1).

Land use and vegetation (USV)

Seven USV coverages were analyzed in vector type format, denominated: Series II, 2001 edition; Series 2.5, 2002 edition; Series III, 2005 edition; Series IV, 2009 edition; Series V, 2013 edition; Series VI, 2016 edition; and Series 6.5, 2017 edition. These series are published by the National Institute of Statistics and Geography (INEGI) and the Mexican Carbon Program and are freely available for download (INEGI, 2019). When plotting the areas covered by the USV types associated with the year of their image, the most noticeable change was observed in 2002 (Series III), with a 22 % reduction in the area of forest (oak plus oak-pine) and a 168 % increase in shrub secondary vegetation (Table 1). For this reason, the distribution and surface areas of Series II were assigned to the period 1980–2001, and, by means of percentage changes by USV in each sub-basin, the differences identified in Series III were incorporated for the period 2002–2017.
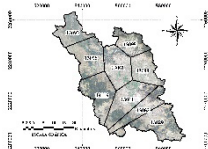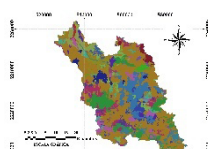
Soil type
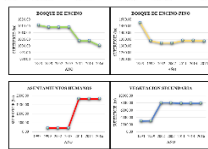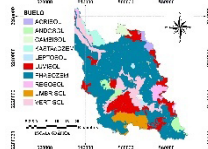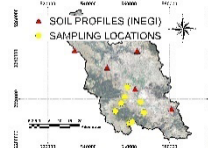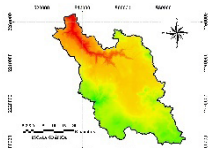
The spatial distribution by soil type was taken from Series II (INEGI, 2014), serving as a complement to the laboratory analysis of 32 soil samples taken at the following depths: 0–40, 40–80, 80–120, and < 120 cm, in eight sites distributed within the basin (two in each of the four soil types that dominate 92 % of its surface: Phaeozem, Luvisol, Vertisol, and Umbrisol). Hydraulic conductivity values associated with the main streams, with variations ranging from 13.74 to 48.1 mm h^{-1}, were measured with infiltration tests using a Guelph model 2800K1 permeameter (ICT International, Australia).

Losses due to water demand for different uses

The volumes concessioned by type of use, currently in the Public Registry of Water Rights (REPDA, 2018), were taken. Once located and differentiated by sub-basin, they were separated by type of source (surface and groundwater). For the estimation of the

Table 1. Characteristics of the SWAT model's information and input data.

Type	Information	Format	Source	Image
Climatological	Precipitation and temperature	csv/txt	Climate Computing Project (CLICOM)	Thiessen polygons
	Solar radiation, dew point temperature and wind speed		Climate Forecast System Reanalysis (CFSR)	
Land Use and Vegetation (USV)	Series II (1993)* Series 2.5 (1999) Series III (2002)* Series IV (2007) Series V (2011) Series VI (2014) Series 6.5 (2016)	Vector (polygon)	USV INEGI scale 1:250 000	
Soil	Edaphological	Vector (polygon)	Edaphology Series II, INEGI, scale 1:250000	
	pH, electrical conductivity, organic matter, texture, bulk density, and moisture content at saturation	txt	Laboratory analysis of soil samples	
		Vector (points with information)	Soil profiles, series II, INEGI, scale 1:250,000.	
Slopes and elevations	Elevation	Raster	Mexican Elevation Continuum (CEM 3.0)	

*USV series used directly within the program, year to which the image corresponds in parentheses. INEGI: National Institute of Statistic and Geography (Mexico).

volume of returns, the Official Mexican Standard NOM-011-CONAGUA-2015 (DOF, 2015) was used as a basis. Both the average daily water removal from the riverbed and the average daily water removal from the shallow aquifer, both in $m^3\ d^{-1}$, were assigned on a monthly basis as appropriate in each sub-basin after subtracting the volume of returns.

Special considerations

The proportion of surface area covered by the aquifers within the Venados basin is: 1317 Valle de Tulancingo 60 %, 1315 Huasca-Zoquital 25 %, and 1314 Metztitlán 15 %, the three of the free type and with availability of -20.93, 9.5, and 9.9 hm^3, respectively. The method selected for the calculation of evapotranspiration was Penman-Monteith (Allen, 2005), and for surface runoff, the USDA Soil Conservation Service (SCS) numerical curve method (Mishra and Singh, 2003).

Calibration and validation

Sensitivity analysis of the parameters was performed with the SWATCUP program. The Sequential Uncertainty Fitting algorithm was selected to find the best-fit parameters, so SUFI-2, of Bayesian structure, was chosen (Ma *et al*., 2022). The Nash Sutcliffe performance indicator (NS) and the coefficient of determination (R^2) were the target functions in the calibration and validation processes for 1982–2002 and 2003–2013, respectively. The equilibrium period, warming, or number of years omitted, was 1980 and 1981.

Hydrological balance

The elements that constitute the soil-water balance equation were determined, which is expressed by an adaptation of the equation of Neitsch *et al*. (2011) that uses daily values, considering monthly values through two proposals. In the first, the water stored in the soil profile (SW) is assumed to be the initial water content, deriving the following equation:

$$SW1_{mi} = SW_{mi} + \Sigma(PREC_{mi} - SURQ_{mi} - ET_{mi} - PERC_{mi} - GW_{mi}) \tag{1}$$

where $SW1_{mi}$ is the final water availability in soil number one, the mean value of month i (mm), and the amount of water in the soil profile at the end of the period (month); SW_{mi} is the initial water content in the soil profile, mean value of month i (mm); $PREC_{mi}$ is the amount of precipitation (rainfall in this case), mean value of month i (mm); $SURQ_{mi}$ is the amount of surface runoff, mean value of month i (mm); ET_{mi} is the amount of evapotranspiration, mean value of month i (mm); $PERC_{mi}$ is the amount of water infiltrating into the soil profile, mean value of month i (mm); and GW_{mi} is the contribution of groundwater or baseflow entering the mainstream, mean value of month i (mm).

For the construction of the present surface approach model, limited subway hydrological information was available, where aquifer 1317 presents a deficit of -20.93 hm^3 yr^{-1} (DOF, 2020). In the second proposal, the nullity of water stored in the soil profile was assumed in the balance equation:

$$SW2_{mi} = SW1_{mi} - SW_{mi} + \Sigma(PREC_{mi} - SURQ_{mi} - ET_{mi} - PERC_{mi} - GW_{mi}) \tag{2}$$

where $SW2_{mi}$, is the final water availability in soil profile number two, the mean value of month i (mm).

Temporal analysis

Temporal variation in water balance elements and water availability was analyzed. After 36 years of modeling (38 years of data minus two years of warming), 12-year subperiods were chosen for each subbasin, for which the final monthly mean soil water availability ($SW1_{mi}$) was estimated in three subperiods: A) from 1982 to 1993, B) from 1994 to 2005, and C) from 2006 to 2017. The Generalized Additive Model (GAM) was used to compare their behavior at the level of monthly mean values. This is a smoothed, non-parametric regression model, which is considered an extension of the Generalized Linear Models (GLM) (Dubos *et al.*, 2022), choosing the Gaussian family for the response variable. The plots and statistical parameters derived from the GAM application were obtained with the help of the ggplot2 and mgcv libraries within the RStudio software (R Core Team, 2022).

RESULTS AND DISCUSSION

Calibration

In the sensitivity analysis to the model fit parameters, it was found that the variables moisture condition curve number 2 (CN2), initial depth in the shallow aquifer (SHALLST), groundwater lag time (GW_DELAY), and depth of water in the shallow aquifer required for return flow (GWQMN) had a significant effect on the results ($p < 0.05$), so their incorporation into the final model resulted in the hydrographs with monthly mean flows estimated in SWAT (Figure 2). When comparing these hydrographs with those observed at the Venados Hydrometric Station, three periods stand out in which the model underestimated the flow during the calibration period, occurring in September 1984, October 1998, and October 1999, whose progressive order in the graph corresponds to numbers 33, 202, and 214, respectively.

The overall performance of the model was adequate according to the statistical indicators, the coefficient of determination (R^2), and the Nash-Sutcliffe index (NS). Both calibration ($R^2 = 0.89$ and $NS = 0.86$) and validation ($R^2 = 0.77$ and $NS = 0.62$) were favorable (Molnar, 2011). Higher calibration and validation parameters were identified than those obtained by Mengistu *et al.* (2019) in arid and semi-arid areas of Southern Africa, which reached R^2 and $NS > 0.71$ for both periods.

Elements of the Balance

The percentage distribution at the sub-basin level of land use and vegetation, as well as soil type (Table 2), is useful for understanding and analyzing the results of the balance elements, highlighting that the predominant land use is agricultural (46.85 %) and the soil type is Phaeozem (45.31 %). The most significant changes during
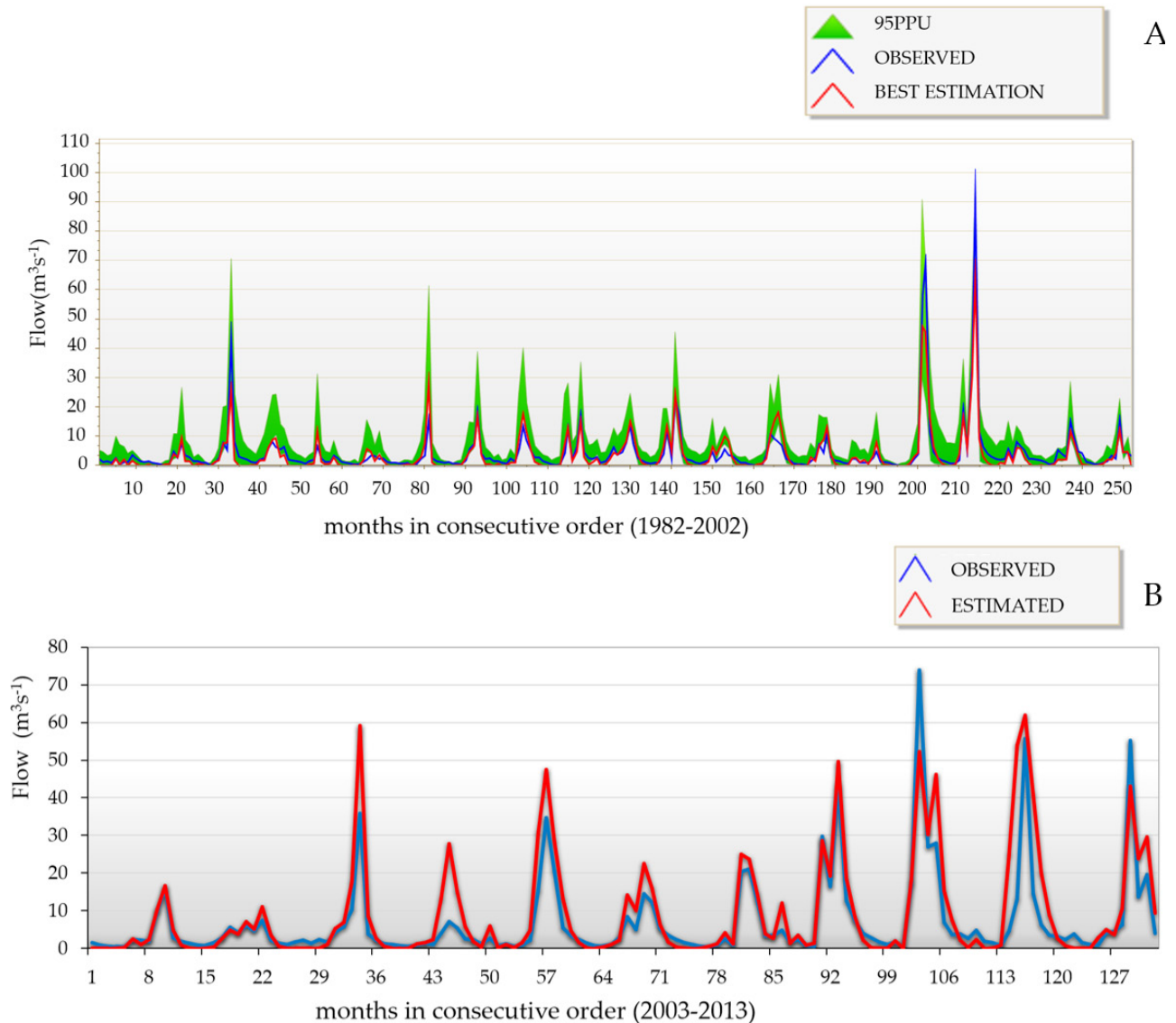
Figure 2. Hydrographs with mean monthly flow values observed at the Venados Hydrometric Station (20° 28′ 2.38″ N, 98° 40′ 15.52″ W), estimated with SWAT, in m^3 s^{-1}. 95PPU: 95 % uncertainty in the prediction. A: calibration period (1982–2002); B: validation period (2003–2013).

the period analyzed (1982–2017) were the 168 % increase in secondary vegetation and the 22 % reduction of the different forest types, as indicated in the model as of 2002. This condition was not considered to have a great impact on the water balance since its changes represent low percentages of the basin's total, 6 and 4 %, respectively. However, the reduction in forest types can potentially impact annual discharge, as suggested by Sharma *et al*. (2022) in a study conducted in the Sabarmati River basin in western India.

Table 2. Land use and vegetation distribution (INEGI Series II,1993), and soil type by sub-basin (in percentage) in the Tulancingo River basin, Mexico (INEGI, 2019).

Land Use and Vegetation	Sub-basin									Total
	5	6	7	8	9	10	11	12	13	
Vsa / Pine-oak B			2.70							0.66
B oak-pine		9.72	5.56			11.03	0.40	8.66	2.84	4.29
Vsa / B for tasteless						1.67		5.25	0.23	0.48
Rainfed and irrigated agriculture	**68.20**	**71.41**	**73.29**	29.03	**73.72**	**51.41**	**66.98**	43.45	**65.95**	**64.85**
B oak		2.12	0.89			10.16		2.32		1.31
Vsa / B oak	6.17	3.39	5.11	0.78		3.79	1.47	0.74		2.55
B pine		3.51	5.30	0.71		20.73	21.14	35.14	18.36	14.08
Vsa / B pine									0.85	0.18
Crassicaule scrub	3.32									0.15
Vsa		1.19								0.11
Induced pasture	3.88	5.80	3.72	21.12			8.78	0.25	7.63	6.06
Urban area	18.43	2.86	3.34	**47.77**	26.28	1.22	1.21	4.18	4.14	5.23
Water body			0.09	0.58			0.02			0.05
Soil type										
Andosol							15.98		0.98	3.98
Leptosol			0.86	10.40	39.44		0.46		1.30	1.10
Luvisol	1.42	0.03	26.44			**51.11**	20.08	17.40	19.39	20.11
Phaeozem	32.41	**64.88**	48.45	55.52		0.41	**46.47**	14.34	**58.25**	**45.31**
Regosol		16.75					7.89			3.43
Umbrisol			13.03			40.93		**59.63**	14.84	12.85
Vertisol	61.45	16.88	11.22	11.94	60.56	7.54	8.97	5.83	4.49	11.71
Urban soil	4.73	1.46		**22.13**			0.14	2.79	0.75	1.51

Vsa: shrub secondary vegetation; B: forest. Underlined values indicate maximum percentages per sub-basin.

When comparing the elements of the water balance at the sub-basin level, it was consistently identified that the highest estimates were associated with the upper sub-basins (11, 12, and 13), whose main streams are the Río Chico (upstream), Ventoquipa Stream, and San Lorenzo River, respectively. On the contrary, the lower values were related to the lower sub-basins (5, 6, 7, 8, 9, and 10), where their main streams are the Tulancingo River (downstream), San Vicente stream, Los Enlamaderos River, Río Chico (downstream), Tulancingo River (upstream), and Camarones stream, in that order (Figure 3). As an example, the element water stored in the soil profile (SW) presented, on average, values of depth 2.8 times higher in the upper sub-basins than those obtained in the lower sub-basins.

The second element of the balance, rainfall (PREC), showed a similar behavior in which the upper sub-basins obtained 220 % more depth height than the lower sub-basins, with a maximum period from May to October and a minimum from November to April. This condition in the rainfall of the present study coincides with what was
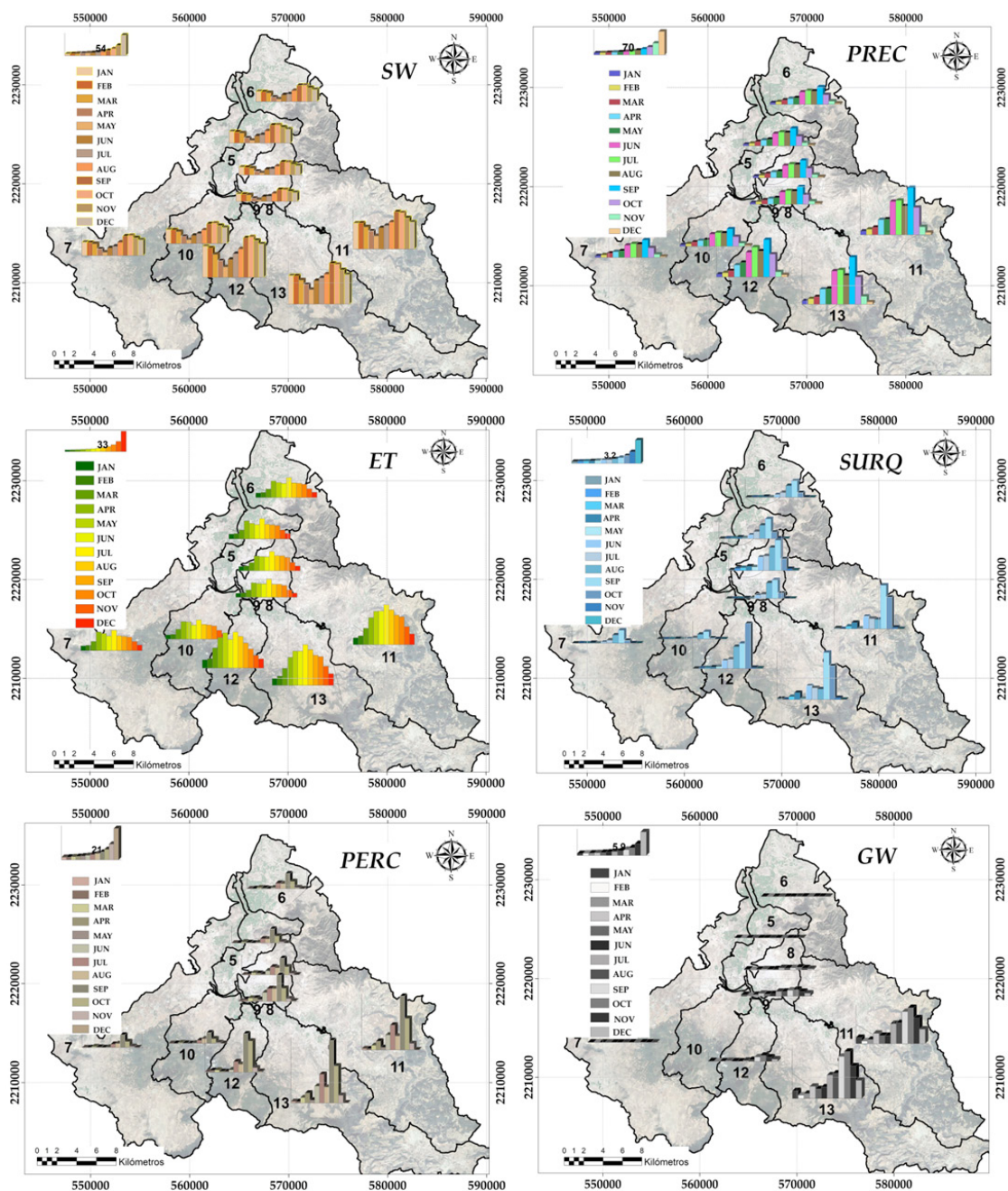
Figure 3. Mean monthly distribution of water balance elements by sub-basin for the 1982–2017 period in the Tulancingo River basin, Mexico. SW: initial soil water content; PREC: precipitation; ET: evapotranspiration; SURQ: surface runoff; PERC: infiltration; GW: baseflow, water depth in millimeters.
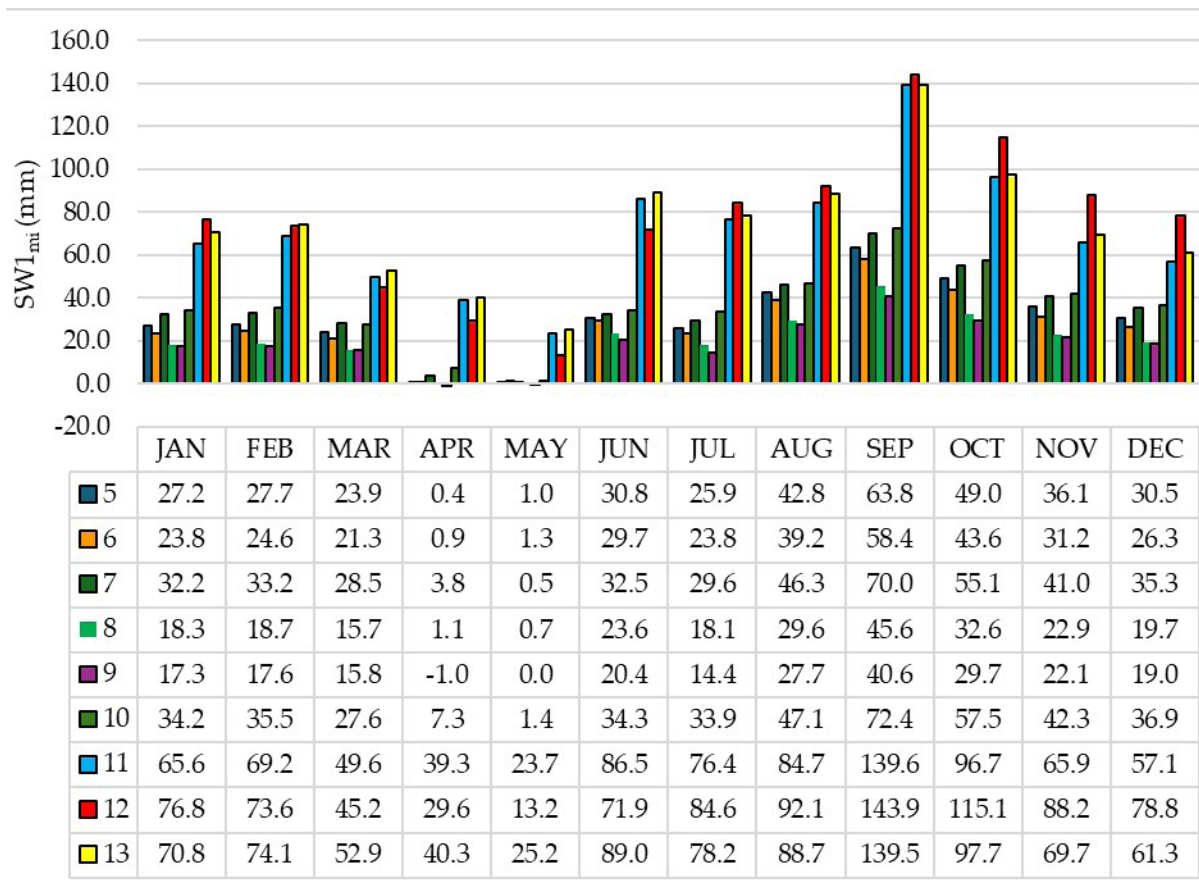
previously reported by Herrera *et al.* (2018), where when analyzing the Tulancingo basin, they grouped the rainy months (May–October) into two periods: May–July and August–October, warning of a high probability of an extreme event in the second one. In relation to the average monthly behavior of the third element, evapotranspiration (ET), it was observed that the maximum levels occur during the summer (July to September), when crop production in Mexico is highest (Monterroso-Rivas and Gómez-Díaz, 2021). This could be associated with evapotranspiration in the agricultural zone, which dominates 64 % of the basin. However, the forest zone in the upper watersheds, which covers 18 to 35 % of its surface, also has an impact on this condition. In fact, both uses in basins 10, 11, and 12 occupy more than 80 % of their surface area, and their average annual average evapotranspiration level is 38.4 mm, 202 % higher than the average evapotranspiration level of the rest of the sub-basins (18.9 mm).

The maximum surface runoff (SURQ) occurred in September, which coincides with the wettest month in all sub-basins. Sub-basins 7 and 10 stand out in this case for their lower runoff. In these areas, the dominance of rainfed and irrigated agriculture, combined with the good porosity of their soils (Phaeozen and Umbrisol), explain the increase in evapotranspiration and, in this case, the reduction of surface runoff (Qiu *et al.*, 2011).

According to Bernal-Santana *et al.* (2022), the characteristics that influence a lower infiltration rate determine the higher runoff rate in a watershed, such as soil permeability or slope. In the Tulancingo watershed, the dominant soil type is Phaeozem (45.3 %), which is characterized by good fertility and porosity (IUSS, 2015) and contributes to the period of maximum infiltration (PERC). However, the period of maximum infiltration coincides with the period of maximum runoff, so it is assumed that it is due to the magnitude of rainfall, so this assertion does not apply in this case. Of the elements analyzed in the balance, sub-basins 11, 12, and 13 showed higher values of rainfall depth, evapotranspiration, and infiltration, reflecting their contribution to baseflow (GW) and highlighting their influence in sub-basins 11 and 13, where the sum of their monthly average values was 250 % higher than the sum in sub-basins 5, 6, 7, 8, 9, 10, and 12. It is in these same sub-basins (5 to 12) that, when the maximum surface runoff occurs, the lowest baseflow depth is generated, similar to what happened in the Awash River in Ethiopia (Shawul *et al.*, 2019).

Surface Balance

The mean monthly final water availability in soil number one (SW1$_{mi}$) showed temporal and spatial variation, accentuated in some months (Figure 4). The time of highest availability was observed in September in sub-basins 11, 12, and 13, in which the estimated rainfall depth was 139.6, 143.9, and 139.5 mm, respectively, exceeding sub-basin 5 (63.8 mm), where the outlet of the Tulancingo basin is located, by a little more than 200 %. The difference is greater (over 300 %) in the sub-basins where the settlements of the city of Tulancingo are located (sub-basins 8 and 9), with depths of 45.6 and 40.6 mm, respectively. This result is attributable to the difference in the

	JAN	FEB	MAR	APR	MAY	JUN	JUL	AUG	SEP	OCT	NOV	DEC
5	27.2	27.7	23.9	0.4	1.0	30.8	25.9	42.8	63.8	49.0	36.1	30.5
6	23.8	24.6	21.3	0.9	1.3	29.7	23.8	39.2	58.4	43.6	31.2	26.3
7	32.2	33.2	28.5	3.8	0.5	32.5	29.6	46.3	70.0	55.1	41.0	35.3
8	18.3	18.7	15.7	1.1	0.7	23.6	18.1	29.6	45.6	32.6	22.9	19.7
9	17.3	17.6	15.8	-1.0	0.0	20.4	14.4	27.7	40.6	29.7	22.1	19.0
10	34.2	35.5	27.6	7.3	1.4	34.3	33.9	47.1	72.4	57.5	42.3	36.9
11	65.6	69.2	49.6	39.3	23.7	86.5	76.4	84.7	139.6	96.7	65.9	57.1
12	76.8	73.6	45.2	29.6	13.2	71.9	84.6	92.1	143.9	115.1	88.2	78.8
13	70.8	74.1	52.9	40.3	25.2	89.0	78.2	88.7	139.5	97.7	69.7	61.3

Figure 4. Mean monthly final water availability in soil number one ($SW1_{mi}$) by sub-basin, in millimeters, in the Tulancingo River basin, Mexico.

proportion of vegetation present in both groups of watersheds, since the upper watersheds have a greater area of forest and shrub secondary vegetation, while the lower watersheds have a greater proportion of induced grassland and settlements. This condition is similar to that of the Luanhe River basin in northern China, where it was identified that the forested area not only increased infiltration and soil water storage but also reduced surface runoff by 11 % (Yang *et al.*, 2019).

The trend when comparing the availability of high basins with low basins was analogous for most of the seasons; however, in April and May, the difference was accentuated. For example, in April, the basin with the highest availability was number 13 with 40.3 mm, while sub-basin 9 presented a deficit (negative value) of -1 mm. The decrease in soil moisture content in the lower basins is associated with the increase in evapotranspirative demand and scarcity of rainfall in that season, in addition to the impermeability that characterizes the soil in the urban area established in basins 8 and 9. According to Puskás and Farsang (2009), these urban land modifications frequently

cause changes in fluvial dynamics, highlighting the modification in soil moisture regimes, so it is expected that phenomena associated with these modifications will be reflected in watersheds 8 and 9.

In the mean monthly final water availability in soil number two ($SW2_{mi}$), which was calculated under the assumption of no initial availability, a deficit (negative values) was observed from November to May, which ranged from -20.81 mm of depth (in December for watershed 13) to -0.31 mm (in February for watershed 10) (Table 3). On the contrary, availability (positive values) was observed from June to September. October showed a mixed performance. This scenario, although unlikely, provides evidence of the importance of initial soil moisture content and warns about the continuation of overexploitation of the 1317 Valle de Tulancingo aquifer. Thus, with rainfall being the only source of supply for the requirements within the basin, it will only be enough to cover four of the eight months. Except for the construction of hydraulic infrastructure for water retention and catchment, the deficit trend could be on the rise.

Table 3. Mean monthly final water availability in soil number two (SW2mi) by sub-basin, in millimeters, in the Tulancingo River basin, Mexico.

Month	Sub-basin								
	5	6	7	8	9	10	11	12	13
Jan	-3.09	-2.62	-2.86	-2.46	-2.45	-2.24	-3.03	-5.55	-4.18
Feb	-1.22	-0.81	-0.93	-1.28	-1.14	-0.31	0.62	-4.02	-0.42
Mar	-2.42	-1.88	-2.75	-2.50	-1.64	-3.83	-8.81	-15.74	-10.69
Apr	-12.86	-10.96	-13.64	-8.89	-9.55	-11.72	-8.42	-14.90	-11.66
May	-5.99	-5.11	-8.38	-5.00	-4.57	-8.50	-11.19	-14.65	-13.44
Jun	12.24	12.20	12.12	8.80	7.70	13.01	30.18	24.19	26.94
Jul	4.08	3.93	5.09	1.59	0.36	7.45	14.01	21.55	8.93
Aug	10.90	10.36	11.33	6.46	6.28	11.45	13.44	16.97	9.40
Sep	16.75	15.99	18.39	11.48	9.02	20.38	41.48	39.41	31.53
Oct	1.32	1.19	2.19	-0.97	-1.70	3.72	1.03	7.96	-7.27
Nov	-5.66	-5.50	-5.91	-5.71	-5.23	-5.46	-16.63	-9.50	-20.81
Dec	-5.61	-5.19	-5.83	-4.87	-4.52	-5.40	-14.26	-9.57	-16.69

Temporal analysis

The Generalized Additive Model (GAM) was applied to each set of monthly mean values of the balance depth variables (Equation 1): PREC, SURQ, ET, PERC, GW, SW, and SW1, in addition to potential evapotranspiration (PET) and water productivity (WYLD), in three time periods (A: 1982–1993, B: 1994–2005, and C: 2006–2017). Such a model provided smoothed trend lines for each analysis period, flexible in the form of the relationships between the explanatory variable (months) and its response (balance depth item under study) (Ouarda *et al.*, 2018). The level of adjustment was considered

positive based on the extent to which its variance is explained by more than 60 % (Table 4), according to the calculated coefficient of determination R^2.

The model best represented the behavior of monthly mean potential evapotranspiration (PET) by presenting a value of $R^2 > 0.9$ in all sub-basins, followed by ET $0.79 < R^2 < 0.95$, SW $0.83 < R^2 < 0.3$, SW1 $0.66 < R^2 < 0.84$, PREC $0.64 < R^2 < 0.81$, GW $0.65 < R^2 < 0.75$, and WYLD $0.61 < R^2 < 0.64$. The presence of empty spaces in the table of coefficients of determination is due to R^2 values lower than 0.6, a condition that was assumed to be an insufficient adjustment of the model to the monthly mean behavior of the variable. The absence of surface runoff observed in each sub-basin (SURQ) and water infiltrating into the soil profile (PERC) is due to the same reason.

Table 4. Coefficients of determination (R^2), obtained from the application of the Generalized Additive Model (GAM) model, for each variable by sub-basin.

Sub-basin		PREC	ET	GW	WYLD	PET	SW	SW1
5	R^2	0.64	0.79	-	-	0.94	0.83	0.71
		C***	AC***			B*	C***	C***
6	R^2	0.64	0.81	0.72	-	0.94	0.84	0.71
		C***	A C***	C***		B*	C***	C***
7	R^2	0.64	0.81	0.72	-	0.94	0.84	0.73
		C***	AC***	C***		B*	C***	C***
8	R^2	0.64	0.84	0.68	-	0.94	0.85	0.71
		C***	AC***	C***		B*	C***	C***
9	R^2	0.64	0.81	0.75	0.61	0.94	-	0.68
		C***	AC***	C***	C***	B*		C***
10	R^2	0.77	0.93	-	0.63	0.94	0.84	0.75
		A*** C**	BC*		C***		C***	C***
11	R^2	0.77	0.93	-	0.63	0.94	0.84	0.67
		A*** C**	BC*		C***		C***	A***
12	R^2	0.81	0.95	-	-	0.94	0.93	0.84
		A***	C*				B*C***	AC***
13	R^2	0.77	0.93	0.65	0.64	0.93	0.84	0.66
		A*** C**	BC*	C***	C***		C***	A***

A: 1982–1993; B: 1994–2005; C: 2006-2017; *$p < 0.05$, **$p < 0.01$, ***$p < 0.001$; PREC: rainfall; ET: evapotranspiration; GW: baseflow; WYLD: water productivity: PET: potential evapotranspiration; SW: initial soil water content; SW1: final soil water availability.

Additional to that proven by Dubos *et al*. (2022), who demonstrated the effectiveness of applying the GAM model to climate data, the significance level obtained in this study for the fit function in the period 2006–2017 (C), mostly $p < 0.001$, indicates that the line describes very well the monthly mean behavior for the variables ET, GW, WYLD, PET, SW, and SW1. It is evident that their increase separates them from the previous periods A and B (Figure 5).

The results obtained show that the response of runoff in relation to rainfall during the three periods analyzed is consistent with studies focused on the analysis of the effects of climate change, such as those of Swain *et al*. (2021) and Xuan *et al*. (2021), where the temporal variation patterns of flow are complementary to those of rainfall. Thus, the lower sub-basins, from 5 to 10, show a significant increase in groundwater availability in the last period of analysis (2006–2017), as a result of the increase in rainfall depth. This situation is congruent with the separation that the last period of available information presents both the Venados Hydrometric Station (2006–2013) and the runoff of sub-basin 1 (2006–2017).
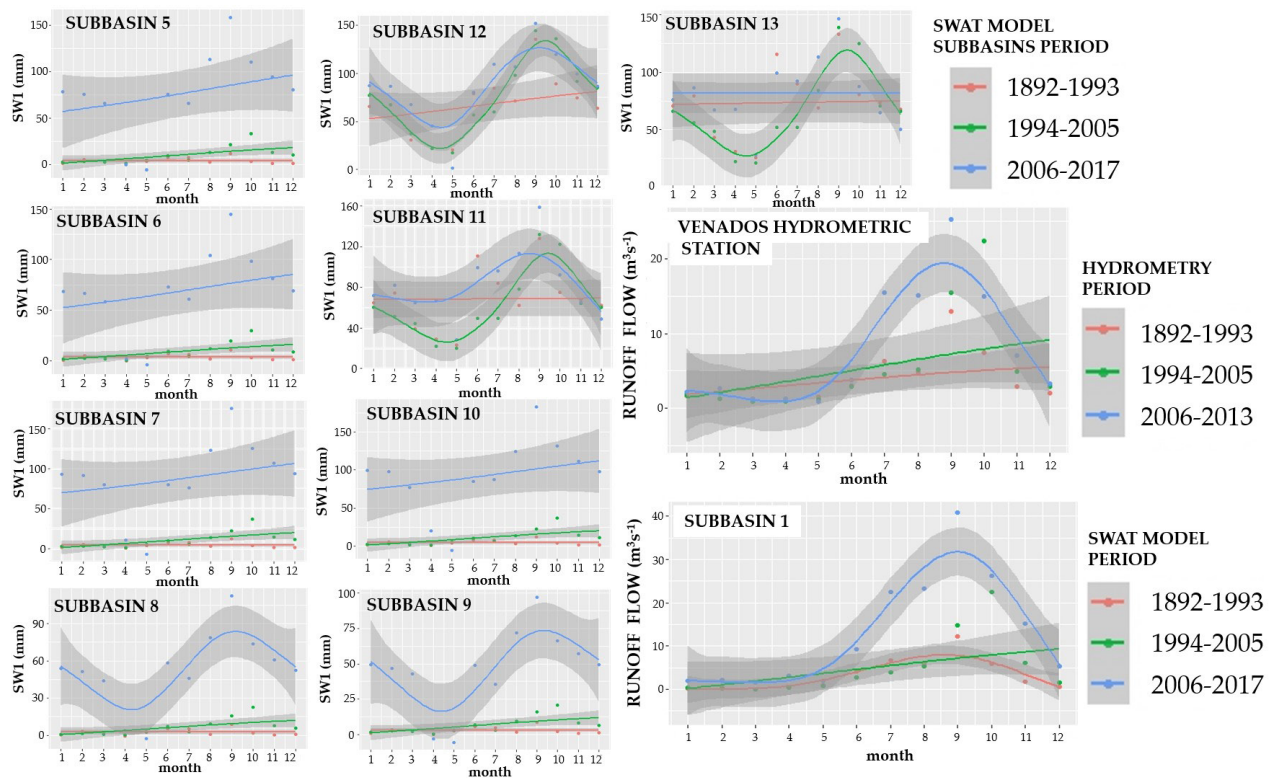
Figure 5. Smoothed trend functions with the Generalized Additive Model (GAM) for mean monthly mean final soil water availability by sub-basin (SW1) (mm); mean monthly runoff flow measured at the Venados Hydrometric Station; and SWAT-estimated flows to the outlet basin (sub-basin 1) (m³ s⁻¹). The gray area indicates a 95 % confidence interval.

CONCLUSIONS

The Generalized Additive Model presented a good statistical fit for most of the hydrologic balance variables ($0.6 < R^2 < 0.94$), so its performance was adequate. In the 2006–2017 period, values notoriously higher than the two previous periods of analysis were observed, identifying a change in the hydrological state of the basin associated

with rainfall in this last period of analysis. Consequently, an analogous change in the surface runoff trend was identified, both in the values modeled with SWAT and those measured at the Venados Hydrometric Station.

Final soil water availability showed a marked spatial and temporal variation. The upper sub-basins had a higher water supply than those located in the lower zone; however, it is in the latter where the largest population is concentrated, as well as the economic activities with the highest demand, mainly agricultural, and therefore, where greater volumes of water are required. In relation to temporal availability, under the scenario of no initial water available in the soil, a water deficit was estimated for most of the year (from October to May) and availability only in the period from June to September. Surface runoff, which is greater in the upper sub-basins during the months of August to October, represents a flood risk in the lower areas, especially considering that in the last period of analysis these differences were accentuated.

The marked differences in water availability, both spatially and temporally, call for the implementation of management actions in the highlands, primarily focused on the conservation and restoration of native vegetation forests to slow runoff, increase aquifer recharge, and reduce peak flows. It is important to manage this resource more efficiently in low-lying areas, mainly those related to agricultural activities, and which correspond to the highest land use in the study basin, in order to prevent a more adverse scenario, similar to that of zero initial soil water availability (SW2).

REFERENCES

Allen R. 2005. Penman-Monteith equation. *In* Encyclopedia of Soils in the Environment. Academic Press: New York, NY, USA, pp: 180–188. https://doi.org/10.1016/b0-12-348530-4/00399-4

Bernal-Santana N, Cruz-Cárdenas G, Silva JT, Martínez-Trinidad S, Moncayo-Estrada R, Estrada-Godoy F, Ochoa-Estrada S, Álvarez-Bernal D. 2022. Variación de la escorrentía superficial por el cambio de uso de suelo en la cuenca del río Duero. Tecnología y Ciencias del Agua 13 (1): 427–469. https://doi.org/10.24850/j-tyca-2022-01-10

Bonasia R, Areu-Rangel OS, Tolentino D, Mendoza-Sanchez I, González-Cao J, Klapp J. 2017. Flooding hazard assessment at Tulancingo (Hidalgo, Mexico). Journal of Flood Risk Management 11 (S2): 1116–1124. https://doi.org/10.1111/jfr3.12312

Dubos V, Hani I, Ouarda TBMJ, St-Hilaire A. 2022. Short-term forecasting of spring freshet peak flow with the Generalized Additive model. Journal of Hydrology 612: 5–11. https://doi.org/10.1016/j.jhydrol.2022.128089

DOF (Diario Oficial de la Federación). 2015. NORMA Oficial Mexicana NOM-011-CONAGUA-2015, que establece las especificaciones y el método para determinar la disponibilidad media anual de las aguas nacionales. Gobierno de México, Secretaría del Medio Ambiente y Recursos Naturales. Ciudad de México, México. https://www.dof.gob.mx/nota_detalle.php?codigo=5387027&fecha=27/03/2015#gsc.tab=0 (Retrieved: January 2023).

DOF (Diario Oficial de la Federación). 2020. ACUERDO por el que se actualiza la disponibilidad media anual de agua subterránea de los 653 acuíferos de los Estados Unidos Mexicanos,

mismos que forman parte de las regiones hidrológico-administrativas que se indican. Gobierno de México, Secretaría del Medio Ambiente y Recursos Naturales. Ciudad de México, México. https://www.dof.gob.mx/nota_detalle.php?codigo=5600593&fecha=17/09/2020#gsc.tab=0 (Retrieved: February 2022).

Herrera E, Magaña V, Morett S. 2018. Relación entre eventos extremos de precipitación con inundaciones. Estudio de caso: Tulancingo, Hidalgo. Nova Scientia 10 (21): 1–19. https://doi.org/10.21640/ns.v10i21.1527

INEGI (Instituto Nacional de Estadística y Geografía). 2014. Mapas edafológicos a escala 1: 250 000, Serie II. México. Instituto Nacional de Estadística y Geografía. Ciudad de México, México. https://www.inegi.org.mx/temas/edafologia/#Descargas (Retrieved: March 2019).

INEGI (Instituto Nacional de Estadística y Geografía). 2019. Mapas de uso de suelo y vegetación a escala 1: 250 000, Series: II, 2.5, III, IV, V, VI y 6.5. Ciudad de México, México. https://www.inegi.org.mx/temas/usosuelo/#Descargas (Retrieved: March 2019).

IUSS (International Union of Soil Sciences). 2015. Base referencial mundial del recurso suelo 2014, Actualización 2015. Sistema internacional de clasificación de suelos para la nomenclatura de suelos y la creación de leyendas de mapas de suelos. Informes sobre recursos mundiales de suelos 106. International Union of Soil Sciences. Roma, Italia. 218 p.

Keller AA, Garner K, Rao N, Knipping E, Thomas J. 2023. Hydrological models for climate-based assessments at the watershed scale: A critical review of existing hydrologic and water quality models. Science of the Total Environment 867: 161209. https://doi.org/10.1016/j.scitotenv.2022.161209

Lopes TR, Zolin CA, Mingoti R, Vendrusculo LG, de Almeida FT, de Souza AP, de Oliveira RF, Paulino J, Uliana EM. 2021. Hydrological regime, water availability and land use/land cover change impact on the water balance in a large agriculture basin in the Southern Brazilian Amazon. Journal of South American Earth Sciences 108: 103224. https://doi.org/10.1016/j.jsames.2021.103224

Ma J, Rao K, Li R, Yang Y, Li W, Zheng H. 2022. Improved Hadoop-based cloud for complex model simulation optimization: Calibration of SWAT as an example. Environmental Modelling and Software 149: 105330. https://doi.org/10.1016/j.envsoft.2022.105330

Marín M, Clinciu I, Tudose NC, Ungurean C, Adorjani A, Mihalache AL, Davidescu AA, Davidescu Șerban O, Dinca L, Cacovean H. 2020. Assessing the vulnerability of water resources in the context of climate changes in a small forested watershed using SWAT: A review. Environmental Research 184: 109330. https://doi.org/10.1016/j.envres.2020.109330

Mendoza-Cariño M, Bautista-Olivas AL, Quevedo-Nolasco A, Mendoza-Cariño D. 2018. Análisis hidrológico de largo plazo en la cuenca del río Metztitlán Hidalgo, México, y su relación con el cambio climático. Hidrobiológica 28 (1): 17–30.

Mengistu AG, van Rensburg LD, Woyessa YE. 2019. Techniques for calibration and validation of SWAT model in data scarce arid and semi-arid catchments in South Africa. Journal of Hydrology: Regional Studies 25: 100621. https://doi.org/10.1016/j.ejrh.2019.100621

Mishra SK, Singh VP. 2003. SCS-CN method. *In* Soil Conservation Service Curve Number (SCS-CN) Methodology. Water Science and Technology Library, vol 42. Springer: Dordrecht, Netherlands, pp: 84–146. https://doi.org/10.1007/978-94-017-0147-1_2

Molnar P. 2011. Calibration. Watershed modelling, SS 2011. Institute of Environmental Engineering, Chair of Hydrology and Water Resources Management. ETH Zurich: Zurich, Switzerland.

Monterroso-Rivas AI, Gómez-Díaz JD. 2021. Impacto del cambio climático en la evapotranspiración potencial y periodo de crecimiento en México. Terra Latinoamericana 39: 1–19. https://doi.org/10.28940/terra.v39i0.774

Neitsch SL, Arnold JG, Kiniri JR, Williams JR. 2011. Soil and water assessment tool, theoretical documentation version 2009. Texas Water Resources Institute: College Station, TX, USA. 618 p.

Ouarda TBMJ, Charron C, Hundecha Y, St-Hilaire A, Chebana F. 2018. Introduction of the GAM model for regional low-flow frequency analysis at ungauged basins and comparison with commonly used approaches. Environmental Modelling and Software 109: 256–271. https://doi.org/10.1016/j.envsoft.2018.08.031

Ortíz-Gómez R, González-Camacho JM, Chávez-Morales J. 2015. Modelo de asignación de agua considerando un caudal ambiental mínimo en la cuenca del río Metztitlán en Hidalgo, México. Agrociencia 49 (7): 703–721.

Puskás I, Farsang A. 2009. Diagnostic indicators for characterizing urban soils of Szeged, Hungary. Geoderma 148 (3): 267–281. https://doi.org/10.1016/j.geoderma.2008.10.014

Qiu GY, Yin J, Tian F, Geng S. 2011. Effects of the «Conversion of Cropland to Forest and Grassland Program» on the water budget of the Jinghe River catchment in China. Journal of environmental quality 40 (6): 1745–1755. https://doi.org/10.2134/jeq2010.0263

R Core Team. 2022. R: A language and environment for statistical computing. R Foundation for Statistical Computing. Vienna, Austria. https://www.R-project.org/ (Retrieved: May 2022).

Ramírez-Cruz H, López-Velasco O, Ibáñez-Castillo LA. 2015. Estimación mensual de intensidad de la lluvia en 30 minutos a partir de datos pluviométricos. Terra Latinoamericana 33 (2): 151–159.

REPDA (Registro Público de Derechos de Agua). 2018. Base de datos de los registros inscritos publicados. Con fecha de corte al 31 de diciembre de 2018. Gobierno de México. Registro Público de Derechos de Agua. Comisión Nacional del Agua. https://app.conagua.gob.mx/consultarepda.aspx (Retrieved: June 2019).

Sharma A, Patel PL, Sharma PJ. 2022. Influence of climate and land-use changes on the sensitivity of SWAT model parameters and water availability in a semi-arid river basin. CATENA 215: 106298. https://doi.org/10.1016/j.catena.2022.106298

Shawul AA, Chakma S, Melesse AM. 2019. The response of water balance components to land cover change based on hydrologic modeling and partial least squares regression (PLSR) analysis in the Upper Awash Basin. Journal of Hydrology: Regional Studies 26: 100640. https://doi.org/10.1016/j.ejrh.2019.100640

Siad SM, Iacobellis V, Zdruli P, Gioia A, Stavi I, Hoogenboom G. 2019. A review of coupled hydrologic and crop growth models. Agricultural Water Management 224: 105746. https://doi.org/10.1016/j.agwat.2019.105746

Swain SS, Mishra A, Chatterjee C, Sahoo B. 2021. Climate-changed versus land-use altered streamflow: A relative contribution assessment using three complementary approaches at a decadal time-spell. Journal of Hydrology 596: 126064. https://doi.org/10.1016/j.jhydrol.2021.126064

Valdez-Lazalde JR, Aguirre-Salado CA, Ángeles-Pérez G. 2011. Análisis de los cambios en el uso del suelo en la cuenca del río Metztitlán (México) usando imágenes de satélite: 1985-2007. Revista Chapingo Serie Ciencias Forestales y del Ambiente 17 (3): 313–324. https://doi.org/10.5154/r.rchscfa.2010.06.041

Xuan W, Xu YP, Fu Q, Booij MJ, Zhang X, Pan S. 2021. Hydrological responses to climate change in Yarlung Zangbo River basin, Southwest China. Journal of Hydrology 597: 125761. https://doi.org/10.1016/j.jhydrol.2020.125761

Yang W, Long D, Bai P. 2019. Impacts of future land cover and climate changes on runoff in the mostly afforested river basin in North China. Journal of Hydrology 570: 201–219. https://doi.org/10.1016/j.jhydrol.2018.12.055